


Prevalence and extent of mitral annular disjunction in structurally normal hearts: comprehensive 3D analysis using cardiac computed tomography

Hiroyuki Toh¹, Shumpei Mori ^{2*}, Yu Izawa¹, Hiroshi Fujita¹, Keisuke Miwa¹, Masataka Suzuki¹, Yu Takahashi¹, Takayoshi Toba¹, Yoshiaki Watanabe³, Atsushi K. Kono³, Justin T. Tretter⁴, and Ken-Ichi Hirata¹

¹Division of Cardiovascular Medicine, Department of Internal Medicine, Kobe University Graduate School of Medicine, Kobe, Japan; ²UCLA Cardiac Arrhythmia Center, UCLA Health System, David Geffen School of Medicine at UCLA, Suite #46-119C, 650 Charles E. Young Dr. South, Los Angeles, CA 90095, USA; ³Department of Radiology, Kobe University Graduate School of Medicine, Kobe, Japan; ⁴Department of Pediatrics, Heart Institute, Cincinnati Children's Hospital Medical Center, University of Cincinnati College of Medicine, Cincinnati, OH, USA

Received 1 December 2020; editorial decision 22 January 2021; accepted 1 February 2021; online publish-ahead-of-print 13 March 2021

Aims

Mitral annular disjunction is fibrous separation between the attachment of the posterior mitral leaflet and the basal left ventricular myocardium initially described in dissected hearts. Currently, it is commonly evaluated by echocardiography, and potential relationships with mitral valve prolapse and ventricular arrhythmia have been suggested. However, controversy remains as its prevalence and extent have not been fully elucidated in normal living subjects.

Methods and results

Systolic datasets of cardiac computed tomography obtained from 98 patients (mean age, 69.1 ± 12.6 years; 81% men) with structurally normal hearts were assessed retrospectively. Circumferential extent of both mitral leaflets and disjunction was determined by rotating orthogonal multiplanar reconstruction images around the central axis of the mitral valvar orifice. Distribution angle within the circumference of the mitral valvar attachment and maximal height of disjunction were quantified. In total, 96.0% of patients demonstrated disjunction. Average distribution angles of the anterior and posterior mitral leaflets were 91.3 ± 9.4° and 269.8 ± 9.7°, respectively. Average distribution angle of the disjunction was 105.1 ± 49.2°, corresponding to 39.0 ± 18.2% of the entire posterior mitral valvar attachment. Median value of the maximal height of disjunction was 3.0 (1.5–7.0) mm. Distribution prevalence map of the disjunction revealed characteristic double peaks, with frequent sites of the disjunction located at the anterior to antero-lateral and inferior to infero-septal regions.

Conclusion

Mitral annular disjunction is a rather common finding in the normal adult heart with bimodal distribution predominantly observed involving the P1 and P3 scallops of the posterior mitral leaflet.

Keywords

Anatomy • Computed tomography • Mitral annular disjunction • Mitral valve

Introduction

Mitral annular disjunction is a separation between the atrial wall-mitral valve junction and the left ventricular attachment,¹ initially described using the dissected hearts. In 1986, Hutchins *et al.*¹ indicated potential relationship between disjunction and floppy mitral

valve using 900 autopsied hearts. However, their finding could not be replicated. Rather it was rebutted by Angelini *et al.*,² who concluded the disjunction was an anatomical variation of the normal morphological characteristics. Although these studies are commonly cited as initial studies related to this peculiar structural anatomy, it is not the case. In 1876, Henle³ had already illustrated disjunction (*Figure 1*)

* Corresponding author. Tel: +1 (310) 794 1717; Fax: +1 (310) 794 6492. E-mail: shumpei@g.ucla.edu

Published on behalf of the European Society of Cardiology. All rights reserved. © The Author(s) 2021. For permissions, please email: journals.permissions@oup.com.

with the term 'Faserring' and 'Filum coronarium' representing 'Fibrous ring' and 'Coronal filament' in English, respectively. This 'Filum coronarium' or 'Filum of Henle' was also referred to by Zimmerman⁴ in 1966 and McAlpine⁵ in 1975 with their own images (Figure 1). McAlpine, by citing both Henle and Zimmerman's publications, preferred to describe disjunction as 'subvalvular segment of the aorto-ventricular membrane' or 'subvalvular membrane',⁵ though. Importantly, all of Henle, Zimmerman, McAlpine, and Angelini *et al.* seemed to show disjunction as normal findings.²⁻⁵ On the other hand, Hutchins *et al.*¹ as well as recent clinical studies using echocardiography,⁶⁻¹³ cardiac magnetic resonance imaging,^{12,14} and cardiac computed tomography,¹⁵ showed potential relationships between disjunction and mitral valve prolapse^{1,2,6-10,12-16} and left ventricular tachyarrhythmia.^{7,12,16} This controversy^{9,17} is, in part, owing to the lack of comprehensive data of three-dimensional (3D) distribution of mitral annular disjunction in normal living hearts. Accordingly, the actual prevalence and extent of mitral annular disjunction has yet to be clarified even in the normal hearts, which prohibits the precise understanding of what is normal and what is abnormal. In this study, we aimed to investigate the prevalence and extent of mitral annular disjunction in the structurally normal adult heart by multiplanar reconstruction of the datasets obtained from cardiac computed tomography.

Methods

Study population

We checked datasets of consecutive 1270 patients (63% men) who underwent cardiac computed tomography between January 2015 and December 2019 in Kobe University Hospital, Japan. Out of these datasets, we excluded 806 patients without systolic images, as disjunction cannot be precisely evaluated during diastole with the opening mitral valvar leaflets (Figure 2).^{6,17} Furthermore, 141 patients with mitral annular calcification, 68 patients with a history of open cardiac surgery, 27 patients with

significant mitral regurgitation, 42 patients with severe aortic valvar stenosis, 14 patients with left ventricular dilatation and/or dysfunction, 8 patients with congenital heart disease, and 66 patients with poor image quality were excluded although they had systolic datasets. As a result, 98 patients were finally enrolled in the analysis. The study was approved by the institutional ethics committee of Kobe University Graduate School of Medicine.

Computed tomography

All acquisitions were performed using commercially available dual-source computed tomographic scanners (SOMATOM Force, Siemens Healthcare, Forchheim, Germany) with a standard protocol of prospective or retrospective electrocardiography-gated cardiac computed tomography. All images were acquired during a deep inspiratory breath-hold, using the parameters of tube voltage of 70–120 kV; tube current modulated with automated exposure control, a gantry rotation of 250 ms, and a temporal resolution of 66 ms. All images were reconstructed at best-systole to obtain optimal images of the coronary arteries. The axial image data were reconstructed by the following parameters: a section thickness of 0.6 mm, an interval of 0.3 mm, a field of view of 24 cm, and a matrix of 512 × 512.

Image reconstruction and measurement

To evaluate the distribution angle of mitral leaflets and disjunction, the mitral orifice plane was carefully set by creating the plane involving the following three points using the multiplanar reconstruction method; infero-septal commissure, supero-lateral commissure, and attachment of the centre of the posterior (or mural) mitral leaflet (Figure 3). Each commissure is important to assess the circumferential distribution of the posterior mitral leaflet as the disjunction is exclusively related to this leaflet. Each commissural point is determined by scrolling the multiplanar left ventricular short-axis image to locate the points where the edge of the anterior (or aortic) mitral leaflet/aortic-to-mitral fibrous continuity becomes apart from the left ventricular outflow tract (Figure 3), with also referring to orthogonal images. These bilateral commissural points approximately correspond to the distal end of both right and left fibrous trigones (Figure 3). After fixing these two points, the last third point is set

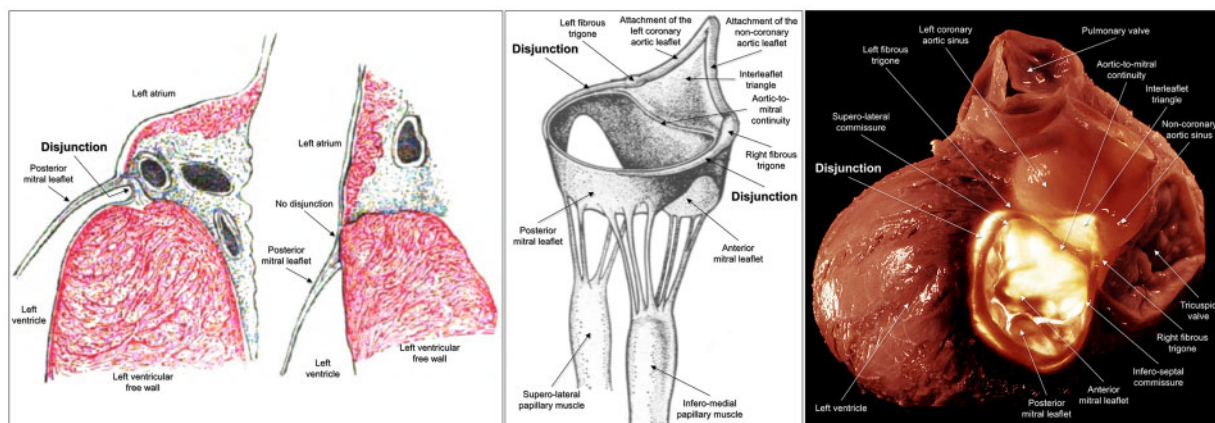


Figure 1 Images from publications of Henle, Zimmerman, and McAlpine. Henle's illustration (left panel) clearly shows samples with (left) or without (right) disjunction. Zimmerman's illustration (central panel) shows lateral and medial disjunctions. McAlpine cited both publications in his textbook. McAlpine's photograph (right panel) demonstrates extensive disjunction using transillumination. Images are reproduced from Refs³⁻⁵ with permissions. All annotations were added by authors. Illustration courtesy of UCLA Cardiac Arrhythmia Center, Wallace A. McAlpine MD collection (right panel).

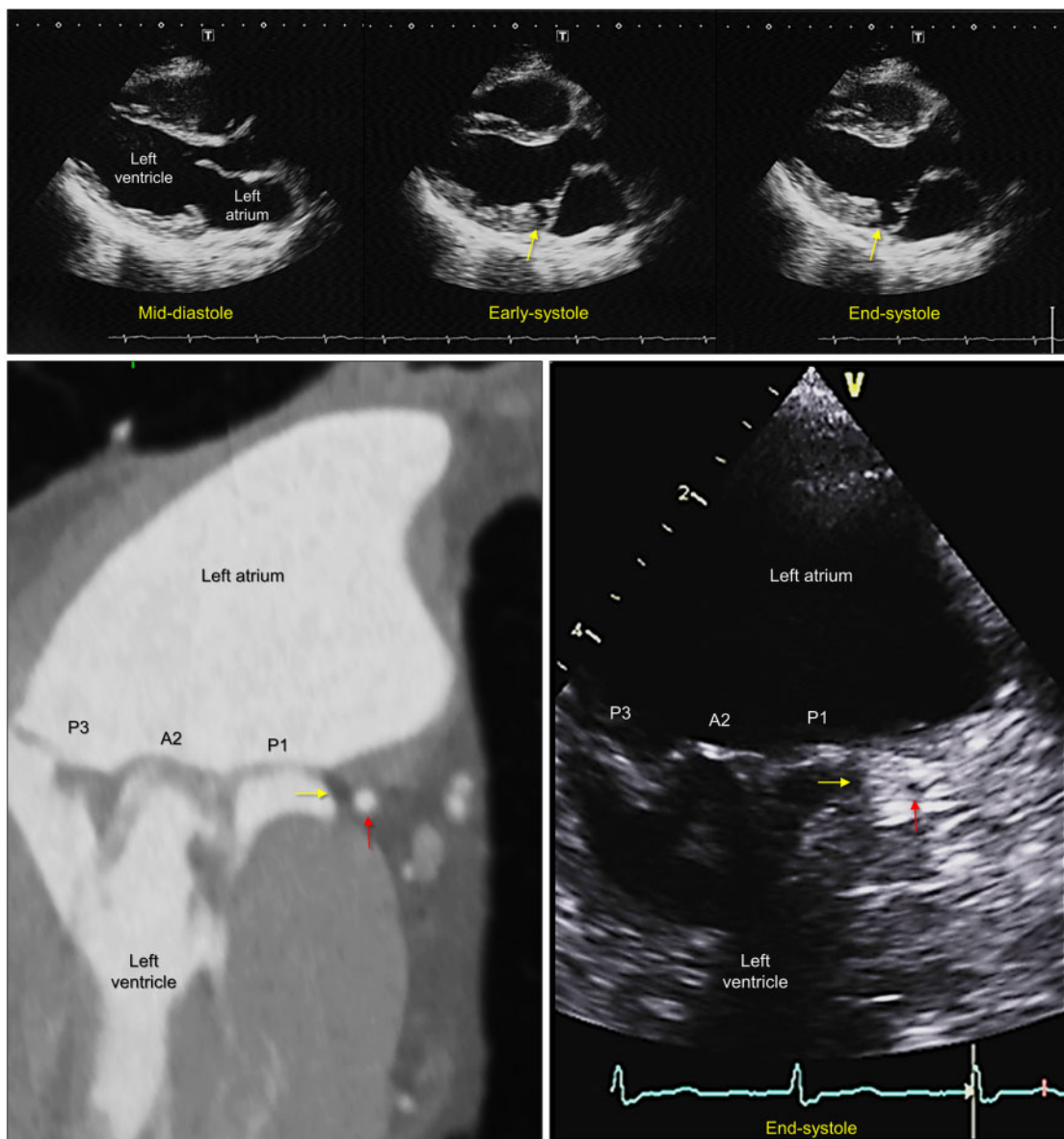


Figure 2 Echocardiographic images of disjunction. Serial transthoracic echocardiographic images (upper panels). Disjunction (yellow arrows) at the infero-lateral region is visible during systole. Lower panels show transesophageal images showing disjunction (yellow arrows) at the subvalvar region supporting the P1 scallop of the posterior mitral leaflet. Red triangles indicate the left circumflex artery. The sectional plane is replicated using cardiac computed tomography obtained from the same patient. The difference in spatial resolution and field of view is evident.

at the attachment of the centre of the P2 scallop to produce the mitral orifice plane as the reference. By estimating an ellipsoid to this fixed mitral orifice plane, the central point was defined. Along the virtual central axis penetrating this central point perpendicularly, orthogonal sections were rotated to observe the entire circumference of the mitral valvar attachment (Figure 3), especially focusing on the posterior mitral leaflet. Disjunction was defined as separation between the attachment of the mitral leaflet and the basal left ventricular myocardium. We measured extent of the disjunction without placing any threshold value as long as it could be detected in those orthogonal sections. The anterior direction of the orthogonal plane bisecting the centre of both commissures was set as

0° with incremental value in degrees along with clockwise rotation. This orthogonal plane to 0° was, therefore, cutting through the aortic root and the infero-lateral free wall of the left ventricle in the opposite 180° direction, showing an image corresponding to the transthoracic echocardiographic parasternal long-axis section. The circumferential extent of the mitral leaflets and disjunction was then determined. When disjunction was observed, the number of disjunction segments with its maximal height were quantified (Figure 3). To assess the distribution pattern of the disjunction, distribution prevalence maps were created by showing the cumulative incidence of the distribution angle in each 0–359° circumference. Long and short radii of the mitral orifice were determined by

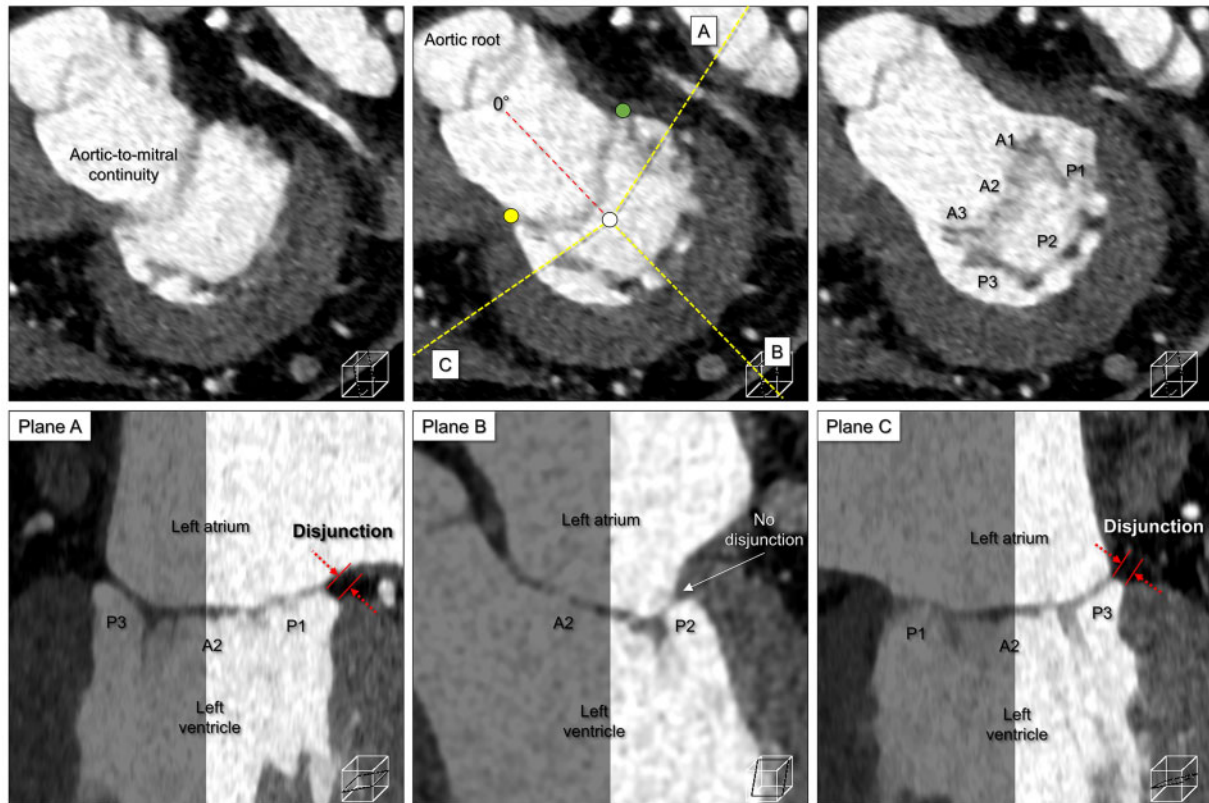


Figure 3 Qualitative measurements of distribution and height of disjunction using computed tomography. Serial multiplanar reconstruction images focusing on short-axis images of the left atrioventricular junction showing the mitral orifice plane (upper middle panel) with its adjacent basal (upper left panel) and apical (upper right panel) planes during systole. The mitral orifice plane was created to involve the supero-lateral commissure (green circle), infero-medial commissure (yellow circle), and centre of the attachment of the P2 scallop. The bilateral commissure point can be determined using these serial images. Yellow dashed line A–C corresponds to multiplanar reconstruction images orthogonal to the mitral orifice plane (lower panels). The white circle indicates the central longitudinal axis of rotation.

measuring the shortest distance between the central point and mitral valvar attachment using multiplanar reconstruction images orthogonal to the mitral orifice plane. Images were analysed using a commercially available workstation (Ziostation2 version 2.4.2.3, AMIN Co., Ltd., Tokyo, Japan, Ziosoft Inc., Tokyo, Japan).

Statistical analysis

Continuous variables with normal distribution and categorical variables are expressed as mean \pm standard deviations and percentages, respectively. Continuous variables with non-normal distribution are expressed as a median (minimum value–maximum value). For the randomly selected 20 patients, intra-observer and inter-observer reliabilities for the measurements of distribution angle of disjunction were assessed by two observers with 4 (H.T.) and 8 (Y.I.) years of experience in analysis of cardiac computed tomographic imaging, and the intra-class correlation coefficient was calculated. All statistical analyses were performed using commercially available software (JMP 11.2.1; SAS Institute, Cary, NC, USA).

Results

At the time of acquisition of images during cardiac computed tomography, the mean heart rate was 73.9 ± 15.1 bpm. Mean

reconstruction phase, mean effective radiation doses, and mean contrast material volume were $32.7 \pm 5.5\%$ of the R–R interval, 12.5 ± 27.7 mSv, and 56.0 ± 24.7 mL, respectively. The clinical characteristics of the patients are listed in Table 1. In the study cohort, the mean age was 69.1 years, 81% of patients were men, and the mean body mass index was 23.4 kg/m^2 .

Table 2 shows computed tomographic measurements. Ninety-four of 98 cases (96%) have disjunction. Mitral annular disjunction was predominantly present at both septal side and lateral side of the posterior leaflet in 78 cases (80%) in continuity with both right and left fibrous trigones, respectively. In 16 cases (16%), disjunction was located at either lateral or septal side. Only four cases (4%) showed no disjunction. The distribution angles, representing the circumferential extent of the structures of interest; of the disjunction, anterior mitral leaflet, and posterior mitral leaflet were $105.1 \pm 49.2^\circ$, $91.3 \pm 9.4^\circ$, and $269.8 \pm 9.7^\circ$, respectively. Distribution angle of the disjunction corresponded to $39.0 \pm 18.2\%$ of entire attachment of the posterior mitral leaflet. Median value of the maximal height of the disjunction was 3.0 (1.5–7.0) mm.

The distribution prevalence map (Figure 4) shows the frequent sites of disjunction. To correlate with echocardiographic

Table 1 Baseline characteristics

Variables	n = 98
Age, years	69.1 ± 12.6
Women, n (%)	19 (19)
Body height, cm	163.3 ± 10.1
Body weight, kg	62.8 ± 13.7
Body mass index, kg/m ²	23.4 ± 3.7
Hypertension, n (%)	61 (62)
Dyslipidaemia, n (%)	63 (64)
Diabetes mellitus, n (%)	34 (35)
Previous percutaneous coronary intervention, n (%)	26 (27)
Previous coronary artery bypass grafting, n (%)	25 (26)
Haemodialysis, n (%)	2 (2)
Atrial fibrillation, n (%)	24 (24)
Indication of cardiac computed tomography, n (%)	
Multiple risk factors	11 (11)
Atypical chest pain	10 (10)
Abnormal electrocardiogram	13 (13)
Effort angina pectoris	18 (19)
Follow-up after percutaneous coronary intervention	8 (9)
Follow-up after coronary artery bypass grafting	17 (17)
Presurgical evaluation (aortic aneurysm)	12 (12)
Preprocedural evaluation (atrial fibrillation)	5 (5)
Others	4 (4)
Background cardiac disease, n (%)	
Normal	45 (46)
Ischaemic heart disease	43 (44)
Valvar heart disease ^a	2 (2)
Others	8 (8)

^aInvolving a case with moderate aortic regurgitation and a case with moderate tricuspid regurgitation.

segmentation of the left ventricle, the plane between the antero-septal and anterior segment is estimated to be 15° clockwise from the original 0° plane. The distribution prevalence map showed a characteristic bimodal shape with frequent sites of disjunction found at the inferior to infero-septal regions (87.8%), followed by anterior to antero-lateral regions (77.5%), and the infero-lateral region (11.2%), in association with the attachment of the posterior mitral leaflet. The long and short radii of the mitral orifice were 18.0 ± 2.0 mm and 12.3 ± 1.8 mm, respectively.

Figure 5 shows representative 3D virtual dissection images showing disjunction at the bilateral attachment of the posterior mitral leaflet, corresponding to the P1 and P3 scallops, reconstructed using computed tomographic data. Attachment of the P2 scallop is located at the infero-lateral left ventricular free wall, with no disjunction. Three-dimensional morphology of the localized disjunction at the P1 scallop took a shape of a subvalvar pocket-like recess (Supplementary data online, Movie).

Figure 6 shows representative gross anatomical and histological images of disjunction prepared from the structurally normal heart, supporting the precision of the observation by Henle in 1876 (Figure 1).

Table 2 Computed tomographic measurements

Variables	
Distribution angle, °	
Mitral annular disjunction	105.1 ± 49.2
Anterior mitral leaflet	91.3 ± 9.4
Posterior mitral leaflet	269.8 ± 9.7
Number of disjunction segment, n (%)	
0	4 (4)
1	16 (16)
2	78 (80)
Maximal height of the mitral annular disjunction, mm	
Septal (range)	3.3 (1.5–7)
Lateral (range)	2.7 (1.5–5.7)
Total (range)	3.0 (1.5–7)
Frequent site of mitral annular disjunction, %	
Anterior to antero-lateral	77.5
Infero-lateral	11.2
Inferior to infero-septal	87.8
Antero-septal	0
Mitral annular diameter, mm	
Long radius	18.0 ± 2.0
Short radius	12.3 ± 1.8

Excellent intra-observer and inter-observer reliabilities were confirmed for the measurements of distribution angle of disjunction, as evident in the values of intra-class coefficients of 0.9987 and 0.9647, respectively.

Discussion

Mitral annular disjunction is characterized by partial separation of the attachment of the posterior mitral leaflet, or mural leaflet of the mitral valve, from the left ventricular myocardium. Whatever terms have been used, including filum coronarium,^{3,4} subvalvular membrane,^{5,18} disjunction,^{1,2,6–17,19,20} subvalvular collar,¹⁸ and subvalvular curtain,²¹ the structural anatomy in topic is a part of the so-called fibrous skeleton of the heart.^{4,18} The anterior mitral leaflet, or aortic leaflet of the mitral valve, is unaffected as it is not related to the left ventricular mural muscular component. Rather, the anterior leaflet is exclusively in continuity with the aortic root by the fibrous aortic-to-mitral continuity,^{22,23} supported by both right and left fibrous trigones bilaterally. This study revealed, first, that mitral annular disjunction was a common finding in normal subjects, observed in 96% of the cohort. Second, the median value of the maximal height of disjunction was 3.0 mm. Third, distribution of the disjunction corresponded to approximately two-fifths of the attachment of the posterior mitral leaflet. Last, the disjunction showed a characteristic bimodal distribution pattern in continuity with bilateral commissures of the posterior mitral leaflet, corresponding to inferior to infero-septal region (P3 scallop), and anterior to antero-lateral region (P1 scallop).

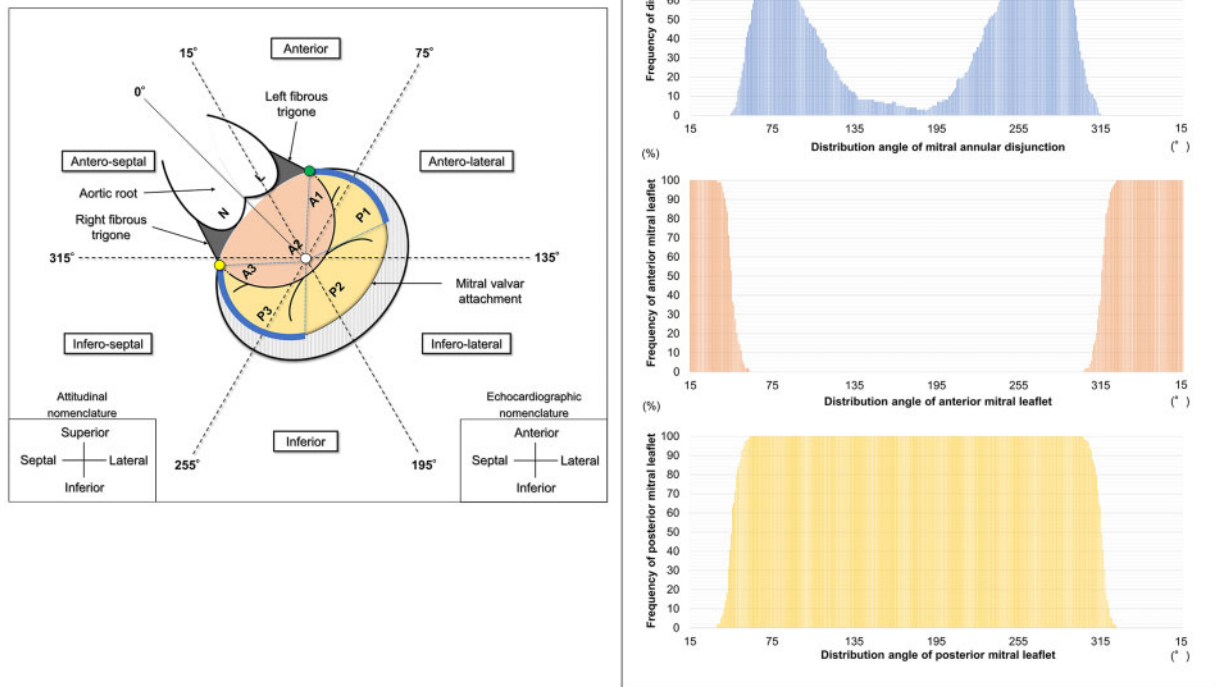


Figure 4 Distribution prevalence map. The left panel shows the schematic diagram of the mitral valvar orifice viewed from the apical direction. The mitral valvar orifice was divided into six segments based on standard echocardiographic segmentation. A plane bisecting the bilateral commissural points was set as 0°. Blue curves suggest representative locations of the bilateral disjunction. Green and yellow circles denote supero-lateral and infero-medial commissures, respectively. The white circle indicates the central longitudinal axis of rotation. The right panels are distribution prevalence maps of disjunction (upper panel), the anterior mitral leaflet (middle panel), and the posterior mitral leaflet (lower panel), showing characteristic double peaks in distribution of disjunction limited to the posterior mitral leaflet.

Measurement of the mitral annular disjunction

In diastole, the diagnosis of disjunction cannot be made because the ventricular myocardium is appropriately situated under the mitral valvar attachment,¹⁷ and the opened leaflet disturbs precise evaluation of the relationship between the posterior mitral valvar attachment and the left ventricular myocardium (Figure 2). During systole, as the myocardium contracts, the disjunction becomes obvious, allowing the precise measurements (Figure 2), from a few millimetres to sometimes more than 1 cm.^{6,17} In the living heart, echocardiography and cardiac magnetic resonance have been commonly used to detect disjunction.^{6–14,16} Although cardiac computed tomography has limitation in dynamic evaluation, its high spatial resolution with wide field of view (Figure 2) merits the precise 3D evaluation. Evaluation using a sectional plane orthogonal to the mitral orifice is particularly important, regardless of either analysis using dissection or living hearts.^{16,17} The parasternal long axis image commonly used to detect disjunction^{7,9,11,13} is nothing but a single plane evaluation of the structure commonly distributed in three-dimensional fashion. It may overlook disjunction, even more so, as the prevalence of disjunction in the

infero-lateral segment is low (Table 2, Figure 4). Without a 3D evaluation, it might be misleading to correlate disjunction with a specific etiology involving the mitral valve or left ventricle.

Controversies in mitral annular disjunction

Although the disjunction itself is not a novel but rather conventional anatomical finding,^{1–5} it has received recent increased focuses, and controversy still arises and/or remains.

The major controversy is the prevalence in normal subjects, which is an important issue to conclude whether disjunction is a pathological finding or not. In contrast to earlier descriptions^{2–5} describing disjunction within the context of normal anatomy, which is supported by the present result with a 96% prevalence, much lower frequencies have been reported as 6.5–37.3% by dissection,^{1,21} 12% by transthoracic echocardiography,^{8,9} 6.7% with 3D transoesophageal echocardiography,¹⁰ and 22% by transthoracic echocardiography or cardiac magnetic resonance imaging.¹²

The extent of its distribution in normal subjects is another potential controversy. We confirmed characteristic double peaks at the

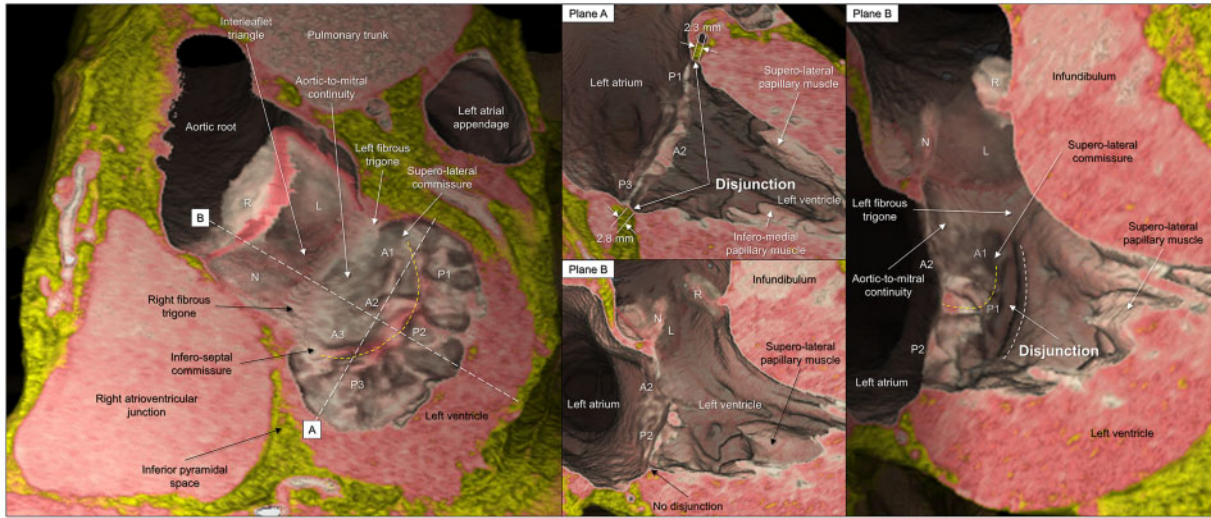


Figure 5 Virtual dissection images showing disjunction. The left panel shows a mitral orifice image viewed from the apical direction during systole. The white dashed lines A and B correspond to the sectional plane A and B in the middle panels. Yellow dashed curves indicate coaptation of the mitral leaflets. The right panel is the sectional plane B viewed from a more apical direction to look into the localized subvalvar recess, created by the lateral disjunction. The white dashed curve denotes the circumferential extent of the lateral disjunction apical to the P1 scallop, which is also evident in the left panel ([Supplementary data](#) online, [Movie](#)). L, left coronary aortic leaflet; N, non-coronary aortic leaflet; R, right coronary aortic leaflet.

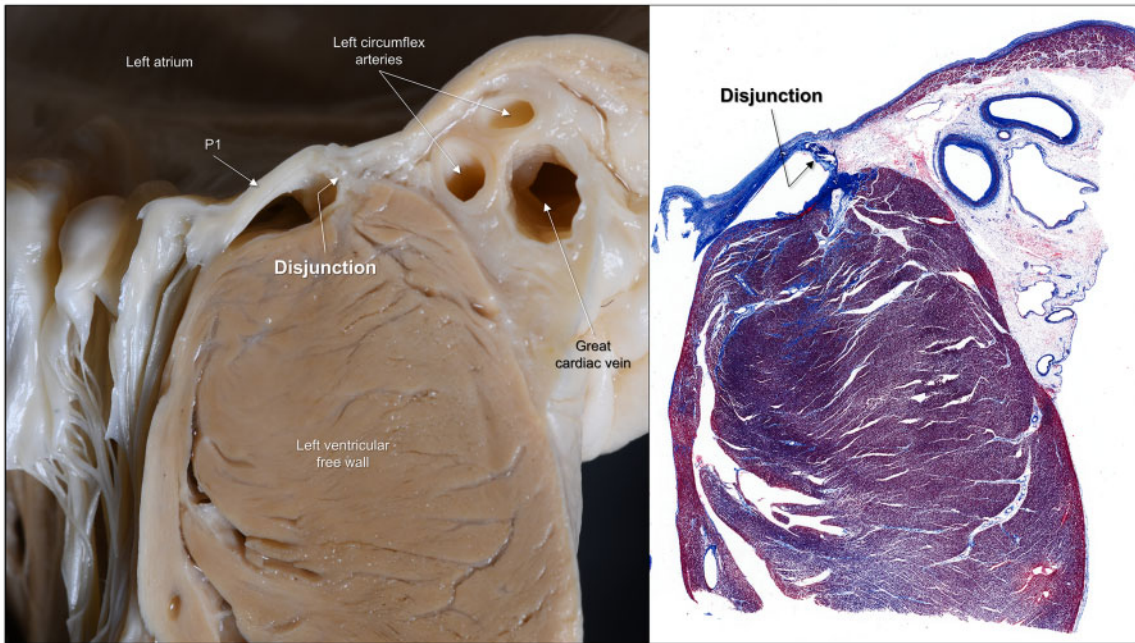


Figure 6 Gross anatomical and histological images of disjunction. Referring to the left panel in Figure 1, these panels show how precise the observation by Henle in 1876 was.

bilateral attachments of the posterior mitral leaflet with an average distribution angle of 105.1° . The bilateral prominent distribution of disjunction is compatible with the description by Henle³ and

Zimmerman.⁴ Henle³ described that the length of the left coronal filament (*Figure 1*), representing lateral disjunction, hits at most about 1/6 of the circumference of the mitral valvar attachment. Nayak et al.²¹

focused on the medial disjunction, which measured 4–21 mm using dissected hearts. The distribution angle of disjunction was reported as 150° by cardiac magnetic resonance¹² and 87° by 3D transoesophageal echocardiography.¹⁰ McAlpine⁵ showed disjunction as a more extensive entity, nearly encircling the entire attachment of the posterior mitral leaflet (Figure 1).

In addition to difference in patients' cohort, various factors, including differences in definition of the disjunction (with or without threshold values), spatial resolution of the measurements, evaluation method (2D or 3D), sample status (cadaveric or living heart), and use of transillumination would affect these diverse results. Thresholds to define the disjunction have been set arbitrarily.^{9,10,12} If the threshold is set higher, the prevalence and extent should be counted lower. Echocardiographic evaluation is generally more challenging due to its limited spatial resolution and field of view. Without evaluation of the entire circumference of the posterior mitral valvar attachment, the prevalence will be underestimated. Even if the entire circumference is focused on, if evaluation was made every 30°,¹² it may not reflect the precise distribution. Evaluation using a dissected heart, including histology, cannot be exactly identical to that of the blood-filled hearts *in situ*. The dissection process itself cannot avoid distortion of the sample. Transillumination may overestimate the extent of disjunction, as is often the case in the evaluation of the membranous septum.

The present result utilizing an imaging modality with superior spatial resolution supports disjunction is a common component of the normal architecture,^{2–5} providing the fibrous basement supporting the hinge of the posterior mitral leaflet. Disjunction rarely encircles the entire attachment of the posterior mitral leaflet^{3–5} as there is no complete ring-like connective tissues supporting the overall attachments of the leaflet.²

Association with mitral valve prolapse

Certain cases with disjunction may be closely linked to mitral valve prolapse,^{1,6–10,12–16} which can be surgically corrected.⁶ Although further investigations without confounding factors are still required,²⁴ mitral valve prolapse and disjunction may also be associated with ventricular arrhythmia.^{7,12,14,16,25} Interestingly, the height of the disjunction with a median value of 3.0 mm in our normal cohort seems to be shorter than that reported in the cases with mitral valve prolapse,^{6,7,9,10} showing an average value of 5.2–10 mm. Furthermore, the height of disjunction is longer in mitral valve prolapse patients with ventricular arrhythmia (8.0 mm) than in those without (6.6 mm).²⁵ Although difference in methods of assessment should be taken into account, this discrepancy may suggest exaggerated disjunction in certain pathological conditions. We have no idea if this potential exaggeration in disjunction height is an acquired or congenital phenomenon, or whether it is also accompanied with change in its distribution angle. Even if such disjunction with extensive height is detected in a 2D single plane, if it has only a few millimetres in its circumferential extent, then it could hardly affect the motion of the corresponding scallop. Three-dimensional distribution and extent, mechanism, optimal threshold value, and natural course of both normal and pathological disjunction need further investigations to both distinguish the two entities as well as figure out optimal strategies to manage a case with mitral valve prolapse combined with pathological disjunction.²⁰ Furthermore, mitral valve prolapse is nothing but a crude classification indicating a characteristic pathological

morphology of the mitral leaflet, potentially involving various underlying conditions affecting the papillary muscles, tendinous cords, mitral leaflets, and/or mitral valvar attachment. For example, therefore, it would not be appropriate to analyze disjunction in cases with fibroelastic deficiency and Barlow's disease within the single context of mitral valve prolapse. Further focus on each background etiology should be required in future studies.

Clinical implications

Anatomically, regardless of its extent, disjunction represents localization of the fibrous thin wall within the high-pressure left ventricle. Thus, it should be a high-risk area during any invasive approach performed involving this region, including radiofrequency catheter ablation,^{26,27} mitral valve surgery,^{28,29} and transcatheter mitral valve replacement.³⁰ Cardiac interventionists and surgeons should be familiar with variation in this anatomy and the relationship to the circumflex coronary artery and coronary sinus. It would be difficult to detect disjunction during any catheter intervention or even in an open-heart surgery with limited field of view. Although the adjacent thick adipose tissue of the atrioventricular groove potentially works as a buffer (Figure 6), damage to this region may induce cardiac tamponade, epicardial hematoma, or submitral left ventricular pseudoaneurysm.^{26–29,31} For example, during the catheter ablation of an accessory pathway or ventricular arrhythmia, getting the catheter stuck within this pocket-like recess (Figure 6) may induce fast increase in tissue temperature combined with significant impedance drop. If higher tissue temperatures are achieved too fast, vaporization with the subsequent gas formation may occur, leading to the steam pop phenomenon,^{26,32,33} which refers to the audible sound produced by intramyocardial explosion when tissue temperature reaches 100°C.³³ This steam pop phenomenon can induce critical complication such as cardiac perforation, even more so if it occurs at the thinner part of the myocardium. In addition to the membranous septum,³⁴ left ventricular outflow myocardium supporting the left coronary aortic sinus,³⁵ left ventricular apex,³⁶ and interleaflet triangles,²² appreciation of the mitral annular disjunction as one of the thin regions within the left ventricle is vital for every cardiac healthcare professionals. Preprocedural analysis of distribution and extent of the disjunction may be indicated to reduce inadvertent complications. Outcome studies focusing on the impact of disjunction on surgical and transcatheter interventions are also required.²⁰

Study limitations

Our study is not without limitations. The single-centre retrospective design, with the need for substantial exclusions, does not allow us to eliminate selective bias. Actually, our final cohort includes women in only 19%. Second, this study was composed of a Japanese population with an average body mass index of 23.4 kg/m². The present values need careful interpretation when compared with non-Asian populations. Third, even cardiac computed tomography may miss the disjunction under its spatial resolution. Last, this study was composed of cases with a structurally normal heart without mitral valvar disease. Investigations of pathological disjunction, if any, are our next topic of investigation.

Conclusions

Mitral annular disjunction was a common finding in patients with normal mitral valves, distributing with characteristic double peaks predominantly observed at bilateral sides of the posterior mitral leaflet. This anatomical information will help improve current appreciation of disjunction and enhance further comprehensive investigations of disjunction found in pathological conditions.

Supplementary data

Supplementary data are available at *European Heart Journal - Cardiovascular Imaging* online.

Acknowledgements

The authors thank the following radiological technologists at Kobe university hospital for their support in the image acquisition and processing: Takuro Nishio, Tomoki Maebayashi, Kiyosumi Kagawa, and Noriyuki Negi. The authors are grateful to Yuki Inoue and Kingo Shichinohe at AMIN Co., Ltd., for their technical support for image reconstruction. The authors appreciate Ann-Kathrin Kahle at Clinic for Cardiology, University Heart & Vascular Center, University Hospital Hamburg-Eppendorf for her translation of German text in Henle's textbook³ into English. The authors wish to thank individuals who donate their bodies and tissues for the advancement of education and research to produce the images in Figure 6.

Data availability

The deidentified participant data generated in this research will be shared on reasonable request to the corresponding author.

Conflict of interest: none declared.

References

- Hutchins GM, Moore GW, Skoog DK. The association of floppy mitral valve with disjunction of the mitral annulus fibrosis. *N Engl J Med* 1986;**314**:535–40.
- Angelini A, Ho SY, Anderson RH, Davies MJ, Becker AE. A histological study of the atrioventricular junction in hearts with normal and prolapsed leaflets of the mitral valve. *Br Heart J* 1988;**59**:712–6.
- Henle J. *Handbuch der systematischen Anatomie des Menschen*. v. 3 pt. 1, 1876. Germany: Vieweg; 1876. p14–20.
- Zimmerman J. The functional and surgical anatomy of the heart. *Ann R Coll Surg* 1966;**39**:348–66.
- McAlpine WA. *Heart and Coronary Arteries: An Anatomical Atlas for Clinical Diagnosis, Radiological Investigation, and Surgical Treatment*. New York, NY: Springer-Verlag; 1975. p956.
- Eriksson MJ, Bitkover CY, Omran AS, David TE, Ivanov J, Ali MJ et al. Mitral annular disjunction in advanced myxomatous mitral valve disease: echocardiographic detection and surgical correction. *J Am Soc Echocardiogr* 2005;**18**:1014–22.
- Carmo P, Andrade MJ, Aguiar C, Rodrigues R, Gouveia R, Silva JA. Mitral annular disjunction in myxomatous mitral valve disease: a relevant abnormality recognizable by transthoracic echocardiography. *Cardiovasc Ultrasound* 2010;**8**:53.
- Clavel M, Hourdain J, Deharo J, Asirvatham SJ, Avierinos J, Ackerman MJ et al. Mitral valve prolapse phenotypes associated with sudden cardiac death. *Can J Cardiol* 2015;**31**:S159–60.
- Konda T, Tani T, Suganuma N, Sumida T, Fujii Y, Kawai J et al. The analysis of mitral annular disjunction detected by echocardiography and comparison with previously reported pathological data. *J Echocardiogr* 2017;**15**:176–85.
- Lee AP, Jin CN, Fan Y, Wong RHL, Underwood MJ, Wan S. Functional implication of mitral annular disjunction in mitral valve prolapse. *J Am Coll Cardiol Imaging* 2017;**10**:1424–33.

- Mantovani F, Benfari G, Clavel MA, Maalouf J, Mankad S, Michelena H et al. Left ventricular consequences of mitral annular disjunction in myxomatous valve disease. *Eur Heart J Cardiovasc Imaging* 2017;**18**:iii52.
- Deigaard LA, Skjølsvik ET, Lie ØH, Ribe M, Stokke MK, Hegbom F et al. The mitral annulus disjunction arrhythmic syndrome. *J Am Coll Cardiol* 2018;**72**:1600–9.
- Konda T, Tani T, Suganuma N, Fujii Y, Ota M, Kitai T et al. Mitral annular disjunction in patients with primary severe mitral regurgitation and mitral valve prolapse. *Echocardiography* 2020;**37**:1716–22.
- Perazzolo Marra M, Basso C, De Lazzari M, Rizzo S, Cipriani A, Giorgi B et al. Morphofunctional abnormalities of mitral annulus and arrhythmic mitral valve prolapse. *Circ Cardiovasc Imaging* 2016;**9**:e005030.
- Putnam AJ, Kebed K, Mor-Avi V, Rashedi N, Sun D, Patel B et al. Prevalence of mitral annular disjunction in patients with mitral valve prolapse and severe regurgitation. *Int J Cardiovasc Imaging* 2020;**36**:1363–70.
- Bennett S, Thamman R, Griffiths T, Oxley C, Khan JN, Phan T et al. Mitral annular disjunction: a systematic review of the literature. *Echocardiography* 2019;**36**:1549–58.
- Enriquez-Sarano M. Mitral annular disjunction: the forgotten component of myxomatous mitral valve disease. *J Am Coll Cardiol* 2017;**10**:1434–6.
- Saremi F, Sánchez-Quintana D, Mori S, Muresian H, Spicer DE, Hassani C et al. Fibrous skeleton of the heart: anatomic overview and evaluation of pathologic conditions with CT and MR imaging. *Radiographics* 2017;**37**:1330–51.
- Ho SY. Anatomy of the mitral valve. *Heart* 2002;**88**:iv5–10.
- Haugaa K. Improving the imaging diagnosis of mitral annular disjunction. *Heart* 2021;**107**:4–5.
- Nayak VM, Victor S. Sub-mitral membranous curtain: a potential anatomical basis for congenital sub-mitral aneurysms. *Indian J Thorac Cardiovasc Surg* 2006;**22**:205–11.
- Mori S, Fukuzawa K, Takaya T, Takamine S, Ito T, Fujiwara S et al. Clinical cardiac structural anatomy reconstructed within the cardiac contour using multidetector-row computed tomography: left ventricular outflow tract. *Clin Anat* 2016;**29**:353–63.
- Mori S, Spicer DE, Anderson RH. Revisiting the anatomy of the living heart. *Circ J* 2016;**80**:24–33.
- Garbi M, Garweg C. Arrhythmia in mitral valve prolapse: all roads lead to Rome. *J Am Coll Cardiol* 2020;**76**:650–2.
- Essayagh B, Sabbag A, Antoine C, Benfari G, Yang LT, Maalouf J et al. Presentation and outcome of arrhythmic mitral valve prolapse. *J Am Coll Cardiol* 2020;**76**:637–49.
- Miura T, Yamazaki K, Kihara S, Saito S, Miyagishima M, Aomi S et al. Transatrial repair of submitral left ventricular pseudoaneurysm. *Ann Thorac Surg* 2008;**85**:643–5.
- Wang H, Zheng Z, Yao L, Mou Y, Wang X. Giant left ventricular pseudoaneurysm: a rare acute complication of radiofrequency catheter ablation for premature ventricular contraction. *J Cardiothorac Surg* 2019;**14**:131.
- Sahan E, Şahan S, Karamanlioğlu M, Gül M, Tüfekçioğlu O. Left ventricular pseudoaneurysm after mitral valve replacement: review of pseudoaneurysms late after mitral valve replacement. *Herz* 2015;**40**:778–82.
- Antonic M, Djordjevic A, Mohorko T, Petrovic R, Lipovec R, Juric P. Left ventricular pseudoaneurysm following atrioventricular groove rupture after mitral valve replacement. *SAGE Open Med Case Rep* 2019;**7**:1–4.
- Blanke P, Dvir D, Cheung A, Levine RA, Thompson C, Webb JG et al. Mitral annular evaluation with CT in the context of transcatheter mitral valve replacement. *J Am Coll Cardiol* 2015;**8**:612–5.
- Frances C, Romero A, Grady D. Left ventricular pseudoaneurysm. *J Am Coll Cardiol* 1998;**32**:557–61.
- Tokuda M, Kojodjojo P, Epstein LM, Koplán BA, Michaud GF, Tedrow UB et al. Outcomes of cardiac perforation complicating catheter ablation of ventricular arrhythmias. *Circ Arrhythm Electrophysiol* 2011;**4**:660–6.
- Viles-Gonzalez JF, Berjano E, d'Avila A. Complications of radiofrequency catheter ablation: can we prevent steam pops? *J Am Coll Cardiol* 2018;**4**:501–3.
- Mori S, Tretter JT, Toba T, Izawa Y, Tahara N, Nishii T et al. Relationship between the membranous septum and the virtual basal ring of the aortic root in candidates for transcatheter implantation of the aortic valve. *Clin Anat* 2018;**31**:525–34.
- Toh H, Mori S, Tretter JT, Izawa Y, Shimoyama S, Suzuki M et al. Living anatomy of the ventricular myocardial crescents supporting the coronary aortic sinuses. *Semin Thorac Cardiovasc Surg* 2020;**32**:230–41.
- Yamamoto K, Mori S, Fukuzawa K, Miyamoto K, Toba T, Izawa Y et al. Revisiting the prevalence and diversity of localized thinning of the left ventricular apex. *J Cardiovasc Electrophysiol* 2020;**31**:915–20.